

## Pseudovector versus pseudoscalar coupling in kaon photoproduction reexamined

S. S. Hsiao,<sup>1</sup> D. H. Lu,<sup>2</sup> and Shin Nan Yang<sup>2</sup>

<sup>1</sup>*Department of Physics, Soo Chow University, Taipei, 11102 Taiwan*

<sup>2</sup>*Department of Physics, National Taiwan University, Taipei, 10617 Taiwan*

(Received 24 November 1999; published 23 May 2000)

The question of pseudovector versus pseudoscalar coupling schemes for the kaon-hyperon-nucleon interaction is reexamined for the reaction  $\gamma p \rightarrow K^+ \Lambda$  in several isobaric models. These models typically include Born terms,  $K^*$  and  $K_1$  exchanges in the  $t$  channel, and a few different combinations of spin-1/2 baryon resonances in the  $s$  and  $u$  channels. The coupling constants are obtained by fitting to a large data set. We find that both pseudoscalar and pseudovector couplings can allow for a satisfactory description of the present database. The resulting coupling constants,  $g_{K\Lambda N}$  and  $g_{K\Sigma N}$ , in the pseudovector coupling scheme are smaller than those predicted using flavor SU(3) symmetry, but consistent with the values obtained in a QCD sum rule calculation.

PACS number(s): 25.20.Lj, 13.60.Le, 13.75.Jz

Kaon electromagnetic production has been studied for more than three decades. However, the progress has not been as swift as in the case of pion production. This is due mostly to the lack of precise experimental data. This is changing as abundant data are coming from various high-energy, high duty cycle electron accelerators like TJNAF, ELSA, and ESRF.

On the theoretical side, most of the calculations have employed the isobar model approach [1–4]. Such an approach includes a limited number of low-lying  $s$ -,  $t$ -, and  $u$ -channel resonances, together with the Born terms, in a fit to data. These phenomenological analyses have been hampered by the fact that many resonances can, in principle, contribute due to the large energy needed to produce a kaon. They differ from each other mostly in the particular set of resonances considered. Despite many persistent efforts to reproduce data [1–4], serious problems remain in the description of kaon production. For example, the coupling constant  $g_{K\Lambda N}/\sqrt{4\pi}$  obtained from the fits by Adelseck-Saghai (AS) [5], Williams, Ji, and Cotanch (WJC) [1] and Mart, Bennhold, and Hyde-Wright [6] are  $-4.17 \pm 0.75$ ,  $-2.38$ , and  $0.51$ , respectively, as compared with the SU(3) value of  $-3.7 \pm 0.7$  [5].

Most theoretical analyses performed so far have employed pseudoscalar coupling (PS) for the kaon-hyperon-nucleon vertex. This is because [7] the use of pseudovector coupling would lead to a further suppression of the leading Born couplings in the fit to data. Another reason is that the value of the coupling constant  $g_{K\Lambda N}/\sqrt{4\pi}$  obtained from the fit within the pseudovector coupling scheme is, in general, considerably smaller than the SU(3) value. However, under flavor SU(3) symmetry, kaon is a member of the pseudoscalar meson octet, as well as the pion and eta meson. Thus, it is natural to expect that the kaon-hyperon-nucleon (KYN) vertex takes the same form as  $\pi NN$ . In the  $\pi N$  system, it is well established that the pseudovector (PV) coupling scheme has an advantage over PS coupling as it respects current algebra and incorporates low-energy theorems. Furthermore, with SU(3) symmetry-breaking effects taken into account, a recent QCD sum rule calculation [8] gave  $g_{K\Lambda N}/\sqrt{4\pi} = -1.96$ , which is only about half of the SU(3) value. We

remind the readers that the result of  $g_{K\Lambda N}/\sqrt{4\pi} = -4.17 \pm 0.75$  obtained by AS [5], which appears to agree well with the SU(3) value, was actually more of a constraint imposed in the fitting. They found many other possibilities within the PS coupling scheme which could give a comparable reduced  $\chi^2$ . It is clear then that the issue is far from being settled. Bennhold and Wright (BW) [9] investigated this question of PV versus PS coupling for the KYN vertex in kaon photoproduction more than ten years ago. They concluded that the data did not prefer one coupling over the other. However, only Born terms were included in the model considered by BW and the fitted data were those available before 1984 which were rather limited. Accordingly, we want to re-address this important question for kaon photoproduction within more extended models and the larger database which is currently available, as recently called for by Bennhold *et al.* [10].

The extended models we considered are similar to those employed by AS [5] and WJC [1]. They consist of Born terms,  $K^*(892)$  and  $K_1(1270)$  exchanges in the  $t$  channel, and a number of spin-1/2 baryon resonances in the  $s$  and  $u$  channels. The kaon-baryon-baryon ( $KBB'$ ) interaction, where  $B$  and  $B'$  can be  $N$ ,  $N^*$ ,  $Y$ , and  $Y^*$ , in either coupling scheme is given as follows:

$$\mathcal{L}_{KBB'}^{PS} = -g_{KB'B} \bar{\psi}_{B'} \Gamma_{\pm} \psi_B \phi_K, \quad (1)$$

$$\mathcal{L}_{KBB'}^{PV} = \frac{f_{KB'B}}{m_K} \bar{\psi}_{B'} \gamma_{\mu} \Gamma_{\pm} \psi_B \partial^{\mu} \phi_K, \quad (2)$$

where  $\Gamma_{+} = i\gamma_5$  and  $\Gamma_{-} = 1$ , depending on whether  $B'$  and  $B$  have the same or opposite parity. As in the  $\pi N$  interaction, the “equivalent” coupling constant for the  $KBB'$  in PV coupling is related to that in PS coupling through the relation

$$\frac{g_{KBB'}}{(m_B + m_{B'})} = \frac{f_{KBB'}}{m_K}. \quad (3)$$

In pseudoscalar coupling, the Born terms are those given in Figs. 1(a)–1(c), while the additional “seagull” diagram of

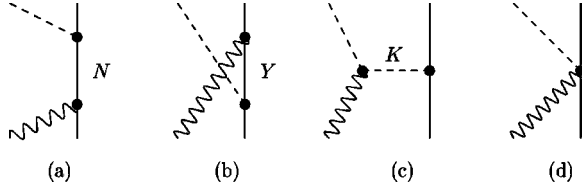
FIG. 1. The Born term diagrams for  $\gamma p \rightarrow K^+ \Lambda$ .

Fig. 1(d) is needed in pseudovector coupling in order to maintain gauge invariance. The couplings of vector mesons  $K^*$  and  $K_1$  with baryons are taken to be a sum of vector and tensor parts, as given in Ref. [11]. With the standard form for the electromagnetic vertices  $\gamma BB'$  and  $\gamma MM'$ , where  $M(M') = K, K^*,$  and  $K_1$  [11], it is straightforward to derive the resulting kaon photoproduction amplitude. Explicit expressions for various amplitudes within the PS coupling scheme can be found in Ref. [11]. In our present calculation, the amplitudes in both PS and PV coupling schemes are evaluated by a computer program which carries out the Dirac algebra in the helicity basis.

The first model (I) we consider is that employed by AS [5] which includes the Roper resonance  $N(1440)$  (N1) and  $\Lambda(1670)$  (L3) in the  $s$  and  $u$  channels, respectively. We follow the notation, e.g., N1 and L3 used above, of Ref. [2] to denote various baryon resonances. In the second model (II), one more resonance  $\Lambda(1405)$  (L1) in the  $u$  channel is added to AS model. As can be seen in Table I, where the meson and baryon resonances included in each model are listed, the third model (III) we study contains four more resonances, i.e.,  $N(1650)$  (N4),  $N(1710)$  (N6),  $\Lambda(1750)$  (L5), and  $\Sigma(1660)$  (S1), than model II.

The fitted data set used in the BW's study of PS vs PV coupling [9] consists of 131 data points for the photon laboratory energy  $E_\gamma$  in the range of 930–1400 MeV, all for the reaction of  $p(\gamma, K^+) \Lambda$ . Of these 131 data points, 108 of them are differential cross sections while the rest are polar-

ization data. In the present study, 242 data points (cross sections and polarization) from the  $\gamma p \rightarrow K^+ \Lambda$  reaction are used in the fitting procedure, as used in the calculation of Ref. [2].

The resulting parameters obtained in the least-squared fit to the data and the  $\chi^2$  per degree of freedom within both PS and PV coupling schemes for the three models described above are listed in Table I. In several cases certain combinations of strong and electromagnetic couplings, e.g.,  $g_{K\Lambda N} \kappa(NN^*)$ , where  $\kappa(NN^*)$  is the transition magnetic moment of  $NN^*$ , always arise together. Therefore, only their product such as  $G_{N^*} = g_{K\Lambda N} \kappa(NN^*)$ , can be determined in the current study as given in Table I. We first repeat the calculation of AS [5], which used PS coupling and fitted to only 117 differential cross section data for the reaction  $p(\gamma, K^+) \Lambda$  available at that time. We find a set of coupling constants which differ slightly from those of their model A but lead to a smaller  $\chi^2/N = 1.21$  as shown in the first column of Table I. We then employ the same model, i.e., including the Born terms and keeping only N1 and L3 resonances but refit to a larger database of 242 data points from the  $p(\gamma, K^+) \Lambda$  reaction. The refitted coupling constants are listed in the column denoted by PS-I. The resulting  $\chi^2/N$  increases to 1.56 since the number of data points considered is considerably larger. Many of the coupling constants obtained differ substantially from the AS values, e.g.,  $g_{K\Lambda N}/\sqrt{4\pi}$  changes from  $-4.11$  to  $-1.55$ . Clearly the selection of database is very important in determining the coupling constants. As demonstrated in Ref. [13], we also find that the coupling constant  $g_{K\Sigma N}$  cannot be determined by the data for the reaction  $\gamma p \rightarrow K^+ \Lambda$  alone (even the sign of  $g_{K\Sigma N}$  may change). The column labeled by PV-I gives the results within the same model I, but with the PV coupling scheme for the  $KBB'$  vertices. It gives an almost identical  $\chi^2/N$  as in PS-I, but the resulting fundamental coupling constants,  $g_{K\Lambda N}/\sqrt{4\pi}$  and  $g_{K\Sigma N}/\sqrt{4\pi}$  decreases by about 20% as compared to PS-I value.

TABLE I. Exchanged particles and associated coupling constants. From the QCD sum rule approach, the leading coupling constants,  $g_{K\Lambda N}/\sqrt{4\pi}$  and  $g_{K\Sigma N}/\sqrt{4\pi}$ , are  $(-2.76, 0.44)$  for the SU(3) symmetric case and become  $(-1.96, 0.33)$  otherwise [8]. Note that  $G_{N^*} \equiv g_{K\Lambda N} \kappa(N^*N)/\sqrt{4\pi}$  and  $G_{Y^*} \equiv g_{KY^*N} \kappa(Y^*\Lambda)/\sqrt{4\pi}$ .

Particle	Coupling	AS	PS-I	PV-I	PS-II	PV-II	PS-III	PV-III
$\Lambda$	$g_{K\Lambda N}/\sqrt{4\pi}$	-4.11	-1.55	-1.24	-1.98	-1.65	-2.41	-1.44
$\Sigma$	$g_{K\Sigma N}/\sqrt{4\pi}$	1.10	0.71	1.04	-0.50	0.36	0.47	0.23
$K^*(892)$	$G_V/4\pi$	-0.44	-0.13	-0.11	-0.14	-0.21	-0.17	-0.17
	$G_T/4\pi$	0.18	0.24	0.37	0.23	0.14	0.09	0.17
$K_1(1280)$	$G_{V1}/4\pi$	-0.10	-0.17	-0.22	-0.17	-0.07	-0.18	-0.12
	$G_{T1}/4\pi$	-1.13	-0.13	-0.07	-0.29	-0.30	-0.36	-0.23
$N(1440)$	$G_{N1}$	-1.43	-1.25	-1.11	-0.97	-1.20	-1.29	-1.10
$N(1650)$	$G_{N4}$						-0.05	0.03
$N(1710)$	$G_{N6}$						0.02	0.01
$\Lambda(1405)$	$G_{L1}$				-0.06	-0.78	-0.08	-0.51
$\Lambda(1670)$	$G_{L3}$	-3.09	-0.09	-1.38	-0.32	-4.81	-0.46	-4.43
$\Lambda(1750)$	$G_{L5}$						-1.81	0.25
$\Sigma(1660)$	$G_{S1}$						-0.42	-0.45
$\chi^2/N$		1.21	1.56	1.57	1.56	1.46	1.38	1.38

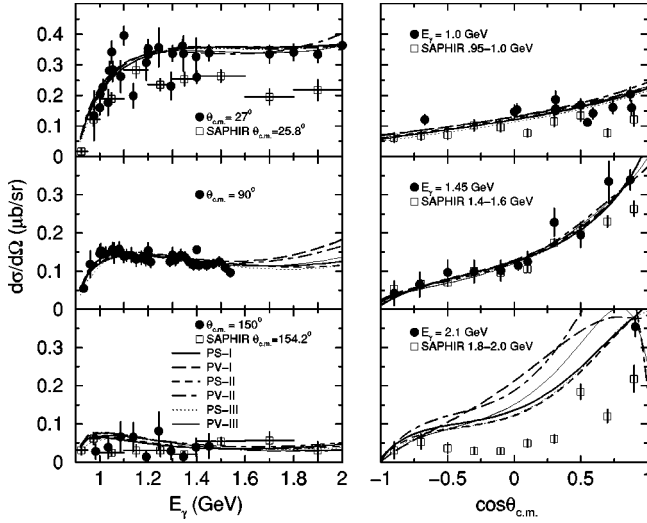


FIG. 2. Differential cross sections for the  $\gamma p \rightarrow K^+ \Lambda$ . The left side shows the energy dependence at  $\theta_{c.m.} = 27^\circ$ ,  $90^\circ$ , and  $150^\circ$ ; the right side gives angular distribution at  $E_\gamma = 1.0$ ,  $1.45$ , and  $2.1$  GeV, respectively. The curves are model calculations for PS-I (solid), PV-I (long-dashed), PS-II (dashed), PV-II (dot-dashed), PS-III (dotted), and PV-III (thin-solid), respectively. The data with filled circles are the same as in Ref. [2]. The data points with open squares are from the SAPHIR collaboration [14].

PS-II and PV-II columns give the results obtained with model II which contains an additional hyperon resonance,  $\Lambda(1405)$  (L1) as compared to model I. The addition of L1 strongly affects other coupling constants, in particular,  $G_{K\Sigma N}$  and  $G_{L3(1670)}$ . As in model I, the coupling constant  $g_{KAN}/\sqrt{4\pi}$  in the PV scheme is smaller than that in the PS scheme. We have tried a number of combinations of baryon resonances in our fitting process. We find that a reasonable  $\chi^2/N$  can be achieved by several different models due to the quality of the present database. A typical result is presented in the last two columns, PS-III and PV-III, of the table. The  $\chi^2/N$ 's obtained with model III become smaller because four more resonances are included.

In Fig. 2 we show the differential cross sections for the above three models as a function of the photon energy (left) and the scattering angle (right). Note that the points with open squares are the latest data from the SAPHIR Collaboration [14] and are not included in our fitting procedure. At lower energies, both PS and PV schemes can provide reasonable descriptions, in other words, the data do not distinguish PS and PV couplings in this region. As the photon energy increases, the theoretical predictions in the PS and PV schemes differ considerably.

In Fig. 3 we show recoil polarization of the  $\Lambda$  with respect to the photon energy (left) and the scattering angle (right). Due to the scarcity of data and large error bars, this quantity gives a small contribution to  $\chi^2$ . As in Fig. 2 the deviations start mainly after  $E_\gamma = 1.3$  GeV. We would like to point out that the present simple model is not able to reproduce the node structure in the angular distribution of the  $P_\Lambda$ , as indicated by the recent data from SAPHIR [14]. Since  $P_\Lambda$  is due to the interference between helicity amplitudes, resonances and final-state interactions play a significant role. A

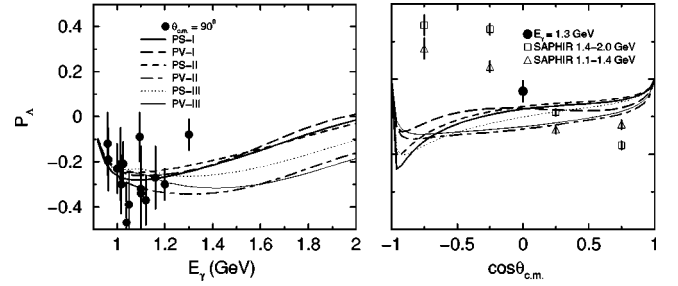


FIG. 3. The  $\Lambda$  polarizations as a function of the photon energy at  $\theta_{c.m.} = 90^\circ$  (left) and a function of  $\cos \theta_{c.m.}$  at  $E_\gamma = 1.45$  GeV (right). The legends for the curves and data are the same as in Fig. 1.

quantitative fit to this observable is possible only with refined models including form factors and final-state interactions. For completeness, we last present the total cross section in Fig. 4. For photon energies below  $1.5$  GeV, both schemes work quite well. To reproduce the higher energy data, it is essential to have hadronic form factors at all interaction vertices [3,12].

Generally, the models with PS coupling give diversified results for the fundamental coupling constants (differing by up to a factor of 3). This implies that the Born terms are not stable with respect to the addition of higher resonances in the PS scheme. In contrast, the fitted results with PV coupling are quite stable toward such additions, and the leading coupling constants in PV schemes are close to each other. Note that the role of  $N(1650)$  emphasized by other groups [3,1,2,13] is not as explicit in our work. The ability to reach a small  $\chi^2$  in most of our cases indicates that the neglect of higher spin resonances (spin-3/2 and higher) is justified in the energy region in which we are interested.

In summary, we have tested the PS and PV schemes for the kaon-baryon interaction in the  $\gamma + p \rightarrow K^+ + \Lambda$  reaction. Our results show that the PV coupling scheme for the kaon-hyperon-nucleon cannot be ruled out by the present database.

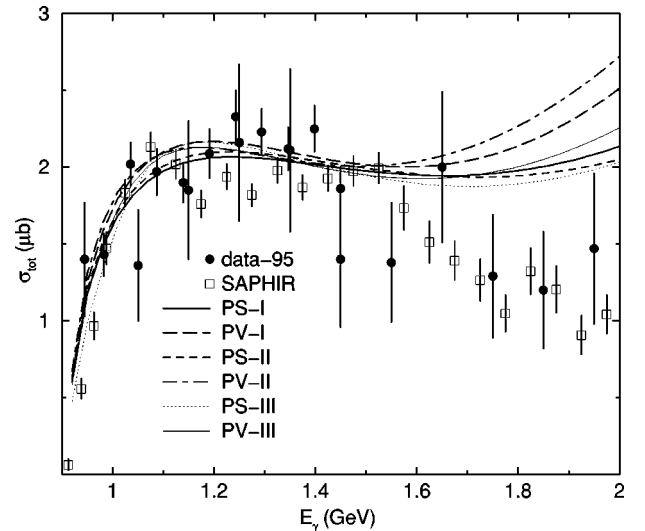


FIG. 4. Total cross sections as a function of the photon energy. The legends for the curves and data are the same as in Fig. 1.

Both schemes can provide reasonable descriptions of the data for the differential cross section below  $E_\gamma=1.5$  GeV. The resulting coupling constants in the PV scheme are somewhat smaller than those from the SU(3) limit, but are consistent with values obtained from a QCD sum rule calculation [8]. To resolve this question, precise data, in particular  $\Lambda$  polarization at backward angles will be helpful, together with a refined theoretical model with a proper treatment of hadron size and final-state interactions.

Another possibility of examining the coupling scheme is the study of kaon photoproduction from nuclear matter. In

this case, whether the leading-order term proceeds through the contact interaction, which only appears in the PV scheme, or not could help to distinguish these two schemes. Any contribution due to the PS coupling must rely on the propagation of the nucleon or the hyperon inside the nuclear medium, which shall manifest itself in the cross sections.

The authors thank B. Saghai for providing them with the data set used in this study and useful discussions. This work was supported in part by the National Science Council of ROC under Grant No. NSC-89-2112-M002-038.

- 
- [1] R. A. Williams, C. R. Ji, and S. R. Cotanch, *Phys. Rev. C* **46**, 1617 (1992).
- [2] J. C. David, C. Fayard, G. H. Lamot, and B. Saghai, *Phys. Rev. C* **53**, 2613 (1996).
- [3] C. Bennhold *et al.*, nucl-th/9901066, to be published in the Proceedings of the Workshop on Electron-nucleus scatterings, Elba, Italy, 1998.
- [4] T. Feuster and U. Mosel, *Phys. Rev. C* **59**, 460 (1999).
- [5] R. A. Adelseck and B. Saghai, *Phys. Rev. C* **42**, 108 (1990); **45**, 2030 (1992).
- [6] T. Mart, C. Bennhold, and C. E. Hyde-Wright, *Phys. Rev. C* **51**, R1074 (1995); C. Bennhold *et al.*, nucl-th/9901066.
- [7] C. Bennhold, *Phys. Rev. C* **39**, 1944 (1989).
- [8] S. Choe, M. K. Cheoun, and S. H. Lee, *Phys. Rev. C* **53**, 1363 (1996).
- [9] C. Bennhold and L. E. Wright, *Phys. Rev. C* **36**, 438 (1987).
- [10] C. Bennhold, T. Mart, and D. Kusno, *Proceedings of the 4th CEBAF/INT Workshop on N\* Physics*, edited by T.-S. H. Lee and W. Roberts (World Scientific, Singapore, 1997), p. 166.
- [11] R. A. Adelseck, C. Bennhold, and L. E. Wright, *Phys. Rev. C* **32**, 1681 (1985).
- [12] Z. P. Li, *Phys. Rev. C* **52**, 1648 (1995); D. H. Lu, R. H. Landau, and S. C. Phatak, *ibid.* **52**, 1662 (1995).
- [13] R. L. Workman, *Phys. Rev. C* **44**, 552 (1991); **39**, 2456 (1989).
- [14] M. Q. Tran *et al.*, *Phys. Lett. B* **445**, 20 (1998).